Transp Porous Med (2017) 116:163–180
DOI 10.1007/s11242-016-0769-9

Unconfined Seepage Analysis Using Moving Kriging Mesh-Free Method with Monte Carlo Integration

Wei Zhang[1,2] · **Beibing Dai**[1,2] · **Zhen Liu**[1,3] · **Cuiying Zhou**[1,2]

Received: 21 January 2016 / Accepted: 14 September 2016 / Published online: 4 October 2016

Abstract The unconfined seepage problem is a classic moving boundary problem, in which the position of phreatic surface is unknown at the beginning of solution and should be determined through iteration. Mesh-free methods are especially suitable for solving this problem. In this work, the moving Kriging mesh-free method with Monte Carlo integration is proposed. Additionally, a corresponding procedure for handling material discontinuity is presented, which extends the approach to inhomogeneous medium. The present method is a true mesh-free method, which does not require a mesh for either shape function construction or numerical integration. Another advantage of the present method is the convenient numerical implementation. Numerical examples show that the present method can achieve better convergence and higher accuracy with rational computation cost when compared with the original mesh-free method. The present method is also verified to be applicable in analyzing transient seepage through homogeneous and inhomogeneous media.

Keywords Mesh-free method · Unconfined seepage · Moving Kriging · Monte Carlo integration · Inhomogeneous earth dam

✉ Cuiying Zhou
ueit@mail.sysu.edu.cn

Wei Zhang
zhangwei3@mail.sysu.edu.cn

Beibing Dai
daibb@mail.sysu.edu.cn

Zhen Liu
liuzh8@mail.sysu.edu.cn

1 Research Center for Geotechnical Engineering and Information Technology, Sun Yat-sen University, Guangzhou 510275, China

2 School of Engineering, Sun Yat-sen University, Guangzhou 510275, China

3 School of Marine Sciences, Sun Yat-sen University, Guangzhou 510275, China

1 Introduction

Unconfined seepage problems exist widely in nature and play an important role, for example, in geotechnical engineering. Due to the complexity of actual problems, numerical approaches are usually adopted to solve them. Since the phreatic surface is unknown at the beginning of solution, there exists difficulty in determining the seepage domain and thus an iteration process is often needed.

There are two categories of approaches for the numerical solution of unconfined seepage problems, the moving mesh approach and the fixed mesh approach. In moving mesh approach (e.g., Crowe et al. 1999), the meshes will be modified during iteration and they are expected to converge at the real location. The main shortcoming is that the meshes must be redefined during iteration and this may cause the aberrant meshes, which limits the application to complicated problems.

Many fixed mesh approaches were developed to overcome this shortcoming. There are two main classes. The first class focuses on the saturated seepage zone, such as the residual flow procedure, the adjusting permeability method. (e.g., Desai 1976; Bathe and Khoshgoftaar 1979; Cheng and Tsui 1993; Jie et al. 2013). The second class is based on saturated and unsaturated theory (e.g., Lam and Fredlund 1984; Lam et al. 1987; Desai and Li 1983; Zhang et al. 2001), in which a suitable pressure–permeability law is required to adjust the parameters of the material. The concept of zero-pressure surface is adopted instead of phreatic surface. There still exist some shortcomings for these methods. In the first class, the elements on phreatic surface, which is also called transition elements, need special treatment in order to obtain satisfactory accuracy. In the second class, the pressure–permeability law is quite difficult to obtain by experiment.

In recent years, many advanced methods were developed for unconfined seepage problems (e.g., advanced approach based on boundary element method (Leontiev and Huacasi 2001; Rafiezadeh and Ataie-Ashtiani 2014), advanced approach based on finite difference method (Bardet and Tobita 2002; Jie et al. 2004), adaptive finite element method (Sharif and Wiberg 2002), mesh-free method (Li et al. 2003; Jie and Liu 2012), variational inequality method (Zheng et al. 2005), moving-mesh finite-volume method (Darbi 2007, Frolkovi 2012), hypersingular equations method (Chen et al. 2007), method of fundamental solutions (Chaiyo et al. 2011), differential quadrature method (Hashemi and Hatam 2011), smoothed fixed grid finite element method (Kazemzadeh-Parsi and Daneshmand 2012, 2013), natural element method (Shahrokhabadi and Toufigh 2013).

Among these methods, mesh-free methods need only the information of nodes, which can be arranged freely. Meanwhile, the approximate field function and its gradient can be continuous in the entire domain. Thus, mesh-free methods are especially suitable for unconfined seepage problems, which are typical moving boundary problems. Some scholars (e.g., Li et al. 2003; Jie and Liu 2012) have solved the unconfined seepage problems using the well-known mesh-free method, the element-free Galerkin method (EFGM) (Belytschko et al. 1994). However, there are two main shortcomings for this approach. Firstly, because the shape functions lack the Kronecker δ function property, it is not easy to accurately impose essential boundary conditions. Secondly, the EFGM is not a true mesh-free method and needs a background mesh for integration. As mentioned above, the transition elements of the background mesh still need special treatment to obtain satisfactory accuracy.

In this work, a novel mesh-free approach for solving unconfined seepage problems is proposed by combining the moving Kriging interpolation and the Monte Carlo integration. The moving Kriging interpolation is adopted for shape functions construction, which has many

advantages (Gu 2003). As it is a passing node interpolation, the constructed shape functions possess the property of Kronecker δ function. So the essential boundary conditions can be directly enforced. In addition, since it is based on the statistics theories for the minimum of mean square error, it can ensure the interpolation accuracy. The global numerical integration is directly performed by the Monte Carlo integration, which is especially suitable for complicated moving phreatic boundary. Additionally, a corresponding material discontinuity handling procedure is presented, which extends this approach to inhomogeneous medium seepage problems. The codes of the present method were developed, and several examples were analyzed to evaluate the present method.

2 Shape Functions Construction Based on Moving Kriging Interpolation

From Gu (2003), the field variable $u(x)$ in the problem domain Ω can be approximated by $u^h(x)$. For any sub domain, the local approximation can be defined by

$$u^h(x) = \sum_{j=1}^{m} p_j(x)a_j + Z(x) = p^T(x)a + Z(x), \tag{1}$$

where $p_j(x)$ are monomial basis functions, a_j are monomial coefficients, and $Z(x)$ is assumed to be the realization of a stochastic process with mean zero, variance σ^2, and nonzero covariance. The covariance matrix of $Z(x)$ is given by

$$cov\{Z(x_i), Z(x_j)\} = \sigma^2 R[R(x_i, x_j)]. \tag{2}$$

In Eq. (2), σ^2 is a scale factor. $R[R(x_i, x_j)]$ is the correlation matrix, and $R(x_i, x_j)$ is the correlation function between any pair of nodes located at x_i and x_j. Many functions can be used as a correlation function $R(x_i, x_j)$; however, a simple and frequently used correlation function is the Gaussian function

$$R(x_i, x_j) = exp\left(-\theta r_{ij}^2\right). \tag{3}$$

in which

$$r_{ij} = \|x_i - x_j\| \tag{4}$$

and $\theta > 0$ represents a value of the correlation parameter used to fit the model. In the paper, $\theta = 0.1$ is taken according to Zheng and Dai (2011). With the implementation of the best linear unbiased estimation, Eq. (1) can be rewritten as follow

$$u^h(x) = p^T(x)\overline{\beta} + r^T(x)R^{-1}(u - P\overline{\beta}), \tag{5}$$

where

$$\overline{\beta} = (P^T R^{-1} P)^{-1} P^T R^{-1} u. \tag{6}$$

The following notations are further employed in this study

$$p(x) = \begin{Bmatrix} p_1(x) \\ p_2(x) \\ \vdots \\ p_m(x) \end{Bmatrix} \tag{7}$$

for $1 \times n$ vector of the known m functions in Eq. (1),

$$P = \begin{bmatrix} p_1(x_1) & p_2(x_1) & \cdots & p_m(x_1) \\ p_1(x_2) & p_2(x_2) & \cdots & p_m(x_2) \\ \vdots & \vdots & \ddots & \vdots \\ p_1(x_n) & p_2(x_n) & \cdots & p_m(x_n) \end{bmatrix} \tag{8}$$

for the $n \times m$ matrix that evaluates function values at the given set of nodes $x_1, x_2, \ldots, x_n$,

$$R[R(x_i, x_j)] = \begin{bmatrix} 1 & R(x_1, x_2) & \cdots & R(x_1, x_n) \\ R(x_2, x_1) & 1 & \cdots & R(x_2, x_n) \\ \vdots & \vdots & \ddots & \vdots \\ R(x_n, x_1) & R(x_n, x_2) & \cdots & 1 \end{bmatrix} \tag{9}$$

for the $n \times n$ matrix of correlation between the $Z's$ (in Eq. (1)) at the given nodes, and

$$r(x) = \begin{Bmatrix} R(x_1, x) \\ R(x_2, x) \\ \vdots \\ R(x_n, x) \end{Bmatrix} \tag{10}$$

for the $1 \times n$ vector of correlation between the given nodes and x.

For simplicity, a $m \times n$ matrix A, and $n \times n$ matrix B are introduced as

$$A = \left(P^T R^{-1} P\right)^{-1} P^T R^{-1} \tag{11}$$

and

$$B = R^{-1}(I - PA) \tag{12}$$

in which I is an $n \times n$ unit matrix, and Eq. (5) can be rewritten as

$$u^h(x) = p^T(x)Au + r^T(x)Bu \tag{13}$$

or

$$u^h(x) = \left[p^T(x)A + r^T(x)B\right]u = \sum_k^n \phi_k(x)u_k, \tag{14}$$

where the shape function $\phi_k(x)$ is defined by

$$\phi_k(x) = \sum_j^m p_j(x)A_{jk} + \sum_i^n r_i B_{ik}. \tag{15}$$

3 Governing Equations for Seepage Problem and Discrete Formulation

3.1 Governing Equations for Seepage Problem

The basic differential equation for transient unconfined seepage in the two-dimensional condition is

$$k_x \frac{\partial^2 H}{\partial x^2} + k_z \frac{\partial^2 H}{\partial z^2} = S_s \frac{\partial H}{\partial t} \tag{16}$$

where k_x and k_z is the hydraulic conductivity, H is the water head, and S_s is the specific storage (1/m), namely the released quantity of storage water caused by compression of medium and expansion of water while water head falls down by one unit in unit volume of saturated medium.

The boundary and initial conditions for Eq. (16) are listed below.

(1) Boundary conditions

Water head:

$$H|_{\Gamma_1} = H(x, z, t) \tag{17}$$

Flux:

$$k\frac{\partial H}{\partial n}|_{\Gamma_2} = q(x, z, t) \tag{18}$$

Phreatic surface:

$$\begin{aligned} H|_{\Gamma_3} &= z \\ k\frac{\partial H}{\partial n}|_{\Gamma_3} &= q = -\mu\frac{\partial H}{\partial t}\cos\theta \end{aligned} \tag{19}$$

(2) Initial conditions

$$H|_{t=0} = H(x, z, 0) \tag{20}$$

where $q(x, z, t)$ denotes the supplied flux in unit area on the flux boundary, q stands for the flux supply caused by alteration of phreatic surface, μ is a dimensionless value called specific yield, and it represents the flux of absorbing (while phreatic surface raises) or discharging (while phreatic surface descends) from unit area of aquifers caused by unit alteration of free surface, and θ is the angle of intersection of outer normal direction of phreatic surface and the vertical line.

3.2 Discrete Formulations

According to the variational principle, the functional of Eqs. (16)–(20) is

$$I = \int\int_{\Omega}\left\{\frac{1}{2}\left[k_x\frac{\partial^2 H}{\partial x^2} + k_z\frac{\partial^2 H}{\partial z^2}\right] + S_s\frac{\partial H}{\partial t}H\right\}\mathrm{d}\Omega + \int_{\Gamma_2\cup\Gamma_3} qH\mathrm{d}\Gamma. \tag{21}$$

According to the interpolation functions presented in Eq. (15), the discrete formulation can be derived as

$$[K]\{H\} + ([S] + [G])\left\{\frac{\partial H}{\partial t}\right\} = \{F\}. \tag{22}$$

The implicit difference is adopted for time discretization, and Eq. (22) can be written as

$$\left[[K] + \frac{1}{\Delta t}([S] + [G])\right]\{H\}_{t+\Delta t} = \{F\} + \frac{1}{\Delta t}([S] + [G])\{H\}_t \tag{23}$$

where,

$$K_{(ab)} = \int_{\Omega}\phi_{a,i}C_{ij}\phi_{b,j}\mathrm{d}\Omega \tag{24}$$

$$S_{(ab)} = \int_{\Omega}S_s(\phi_a\phi_b)\mathrm{d}\Omega \tag{25}$$

$$G_{(ab)} = \int_{\Gamma_3}\mu(\phi_a\phi_b)\cos\theta\mathrm{d}\Gamma \tag{26}$$

$$F_{(a)} = \int_{\Gamma_2}q\phi_a\mathrm{d}\Gamma \tag{27}$$

where a and b are the nodes utilized for local approximation, namely the influence-domain nodes, ϕ_a is the shape function of the node a defined by Eq. (15), and C_{ij} is the hydraulic conductivity.

For the steady seepage problem, substituting $\Delta t = \infty$ into Eq. (23), the discrete formulation can be derived as

$$[K]\{H\} = \{F\}. \tag{28}$$

For the unconfined seepage problem, the solutions of Eqs. (23) and (28) need iteration to satisfy phreatic surface boundary conditions (Eq. (19)). The iteration convergence condition in the paper is given as

$$e = \frac{||H^{(k)} - H^{(k+1)}||_2}{||H^{(k+1)}||_2} < \in \tag{29}$$

where $\in$ is the convergence precision.

4 Numerical Implementation

4.1 Monte Carlo Integration

The Monte Carlo method obtains solutions of mathematical problems by using statistical sampling theory. It is based on the law of large number in probability theory and is promising in many aspects. The Monte Carlo method provides a simple approach to implement numerical integration called Monte Carlo integration. For the integration

$$I = \int_a^b f(x)\mathrm{d}x, \tag{30}$$

the value of I can be considered to be the product between $(b - a)$ and the average value of $f(x)$ over $[a, b]$. The average value of $f(x)$ can be obtained by generating a random sample $x_1, \ldots, x_n$ that is uniformly distributed over $[a, b]$. Thus, we have:

$$\widehat{I} = (b - a)\frac{f(x_1) + f(x_2) + \cdots + f(x_n)}{n}. \tag{31}$$

If $n \to \infty$, $\widehat{I}$ will converge to I with the probability 1. The error in the integration is proportional to the standard error of $\widehat{I}$ and is inversely proportional to $\sqrt{n}$, so we can achieve arbitrary accuracy by adjusting the number of sampling points.

The Monte Carlo integration needs sufficient sampling points, which increases its computation cost in contrast to the Gaussian integration. However, with the development of computer hardware, the computation cost has become less and less important in most cases, and the Monte Carlo integration has become more and more attractive due to its simplicity, adaptability, and independence of the problem dimension (Jie et al. 2013).

To implement numerical integration over the problem domain Ω, we firstly generate a large number of randomly distributed integration points covering Ω. The global shape of integration points is chosen to be rectangle for easy realization. Then looping is performed with respect to all the points in Ω, to implement global numerical integration. Thus, the global permeability matrix $[K]$ in Eqs. (23) and (28) can be calculated as

$$K = \frac{A}{n_{\mathrm{mc}}}\sum_{i}^{n_{\mathrm{mc}}} K_i \tag{32}$$

where A is the global area of randomly distributed integration points, n_{mc} is the number of integration points, and K_i is the stiffness matrix of the integration point i, which can be obtained by Eq. (24). The matrix $[S]$ in Eq. (23) can be calculated in a similar way.

As the problem domain Ω is changeable during the iterations, we only need to determine whether each integration point is in Ω or not, without changing the position of each integration point. The numerical implementation is quite convenient. Thus, the integration approach is especially suitable for complicated moving phreatic boundary. Note that the integration approach is dimensionless, so it is easy to be extended to three-dimensional problems.

For traditional Gauss integration over background mesh (e.g., the EFGM), we need special treatment for the changeable Ω. One option is to modify background mesh during iteration, and another choice is to handle the transition background elements to obtain sufficient accuracy. The present approach abandons the background mesh and can be implemented over the changeable Ω in a concise way with higher accuracy, and this is the main advantage.

4.2 Nodal Connectivity

The nodal connectivity is enforced via mesh in mesh-based methods, such as finite element method, finite volume method, and finite difference method. In mesh-free methods, the nodal connectivity is enforced via the concept of influence-domain. The influence-domains are determined by searching for adequate nodes within a partition P_I in the problem domain Ω, $P_I \subseteq \Omega$ for each integration point. The set of nodes inside the partition P_I , which contributes to the interpolation of the integration point x_I , is called influence-domain.

In the present method, the nodal distribution is dependent on problem domain Ω. As the problem domain Ω is changeable with the moving phreatic surface, the phreatic surface is explicitly represented by some nodes. The nodal distribution can be arranged and changed freely during iteration. Thus, the problem of mesh distortion in mesh-based methods is avoided.

The field nodes and Monte Carlo integration points are connected via the concept of influence-domain. In this paper, the circular influence-domain is adopted with a radius of $2.5d_{\mathrm{c}}$, in which d_{c} is the average nodal distance.

4.3 Material Discontinuity Handling Procedure

In engineering practice, the inhomogeneous medium seepage widely exists. In mesh-free method, there is no mesh of elements, and hence the material interface cannot be defined based on elements. Therefore, special treatment is needed, such as “visibility criterion” and “diffraction method”. (Belytschko et al. 1996a, b; Organ et al. 1996).

In this paper, a corresponding material discontinuity handling procedure is presented. First, the problem domain Ω is divided into several sub domains according to the material zones (Fig. 1a), and the field nodes are divided into several groups accordingly, with a set of nodes in the interface belonging to both material zones. When searching the influence-domain for each integration point, the points in one material can only be influenced by the nodes in this material zone. As shown in Fig. 1b, for integration point A in the material zone Ω_1, if the material discontinuity is not taken into consideration, the point n_1 is the influence point. On the other hand, if the material discontinuity is considered, the node n_1 is not the influence point, since they do not belong to the same material zone. However, the node n_2 is the influence point of integration point A, as n_2 belongs to both material zones. The algorithm proposed in this paper essentially handles the material discontinuity problem by distinguishing the influence-domain of the nodes in different material zones.

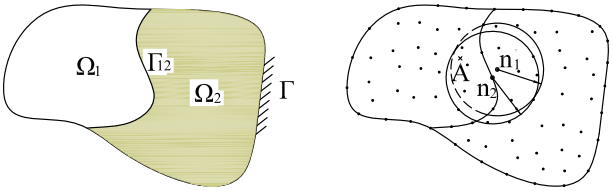

Fig. 1 **a** Material discontinuity problem; **b** material discontinuity handling

Table 1 Numerical procedure for unconfined seepage problems

(1) Generate Monte Carlo integration points covering Ω
(2) Assume an initial phreatic surface
(3) Loop over the time steps (if the transient seepage is considered)
(4) Generate field nodal distribution according to the phreatic surface
(5) Loop over Monte Carlo integration points
  1. Determine the material zone of current integration point.
  If current integration point is not belonging to any material zone,
  exit current point and move to the next point
  2. Determine the influence-domain of current integration point
  3. Compute shape functions and their derivatives
  4. Compute permeability matrix of current integration point
  5. Assemble the contribution of current integration point to global permeability matrix $[K]$ by Eq. (32)
  6. Assemble the contribution of current integration point to the matrix $[S]$
(6) End looping over Monte Carlo integration points
(7) Implement boundary conditions and form global system equation by Eqs. (23) or (28)
(8) Solve the global system equation to obtain the nodal water head result.
(9) Determine whether the result is convergent or not
  If it is convergent, go to the next step. If not, modify the phreatic surface
  according to the head results and goto step (4)
(10) Obtain the gradient and other interesting results
(11) End looping over the time steps (if the transient seepage is considered).

4.4 Numerical Procedure for Unconfined Seepage Problems

The numerical procedure for unconfined seepage problems is given in Table 1.

5 Examples

5.1 Seepage Through a Homogeneous Rectangular Dam

Consider a homogeneous dam with rectangular cross section. The problem is described in Fig. 2a. This is one of the few examples that have analytical solutions in the unconfined seepage analysis (Zheng and Liu 2015). Considering that the analytical formulas are too

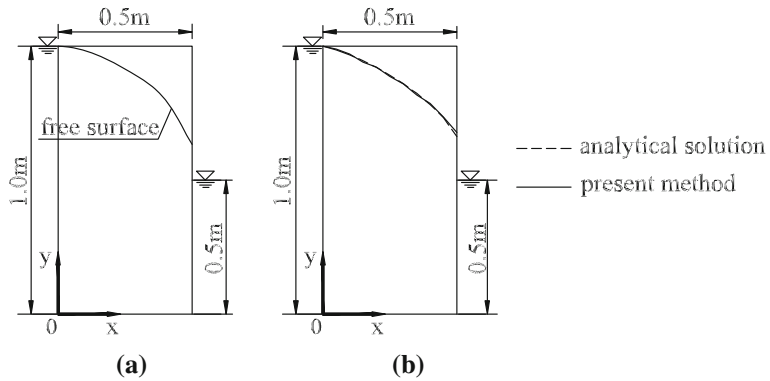

Fig. 2 **a** Seepage through homogeneous rectangle dam; **b** free surface results

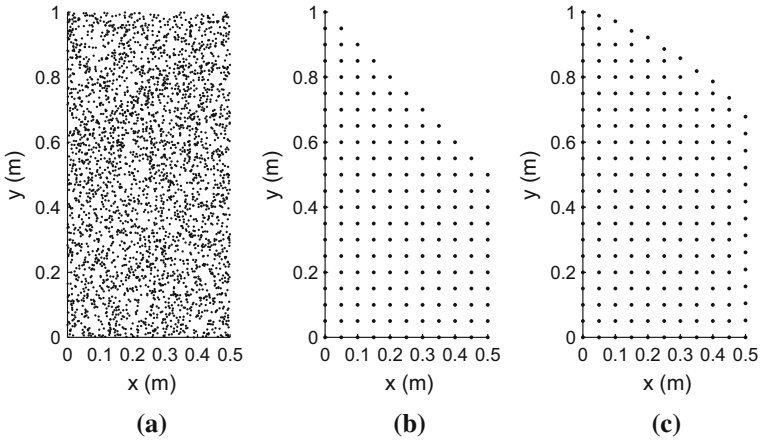

Fig. 3 **a** Monte Carlo integration points; **b** initial nodal distribution; **c** final nodal distribution

complicated to provide results straightforwardly, Hornung and Krueger (1985) gave accurate results in the form of tables and graphs by solving these formulas numerically.

The Monte Carlo integration points and initial and final nodal distributions are shown in Fig. 3. The nodal distance in each direction is 0.05 m. The number of integration points n_{mc} in Eq. (32) was taken to be 3200, and the convergence precision $\in$ in Eq. (29) was taken to be 0.001. The initial nodal distribution is arranged according to an assumed phreatic surface, while the final nodal distribution is modified step by step during iterations based on the present algorithm. It should be noted that the total numbers of nodes during iteration process vary with the location of the phreatic surface.

It is found that the final nodal distribution, which represents the real seepage domain and phreatic surface, is independent of the initial assumed nodal distribution. That is to say, given arbitrary initial nodal distribution, the final nodal distribution converges at almost the same result. The free surface result is compared with the analytical solutions given by Hornung and Krueger (1985) in Fig. 2b and Table 2, and good agreement can be seen. The correctness of the present method is thus validated.

In order to study the influence of the parameters n_{mc} and $\in$ on the performance of the present method, a parametric study has been conducted. Furthermore, in order to compare the

Table 2 Coordinate of some points on the phreatic surface by using the present method and comparing them with the analytical solutions

x (m)	y (m) Analytical	y (m) Present	Error (%)	x (m)	y (m) Analytical	y (m) Present	Error (%)
0.00	1.000000	1.000000	0.000	0.30	0.859969	0.858999	0.113
0.05	0.986242	0.988708	0.250	0.35	0.823876	0.817981	0.715
0.10	0.967625	0.971340	0.384	0.40	0.782493	0.785957	0.443
0.15	0.945590	0.940710	0.516	0.45	0.733142	0.735981	0.387
0.20	0.920382	0.922291	0.207	0.50	0.662382	0.678084	2.371
0.25	0.891939	0.887004	0.553				

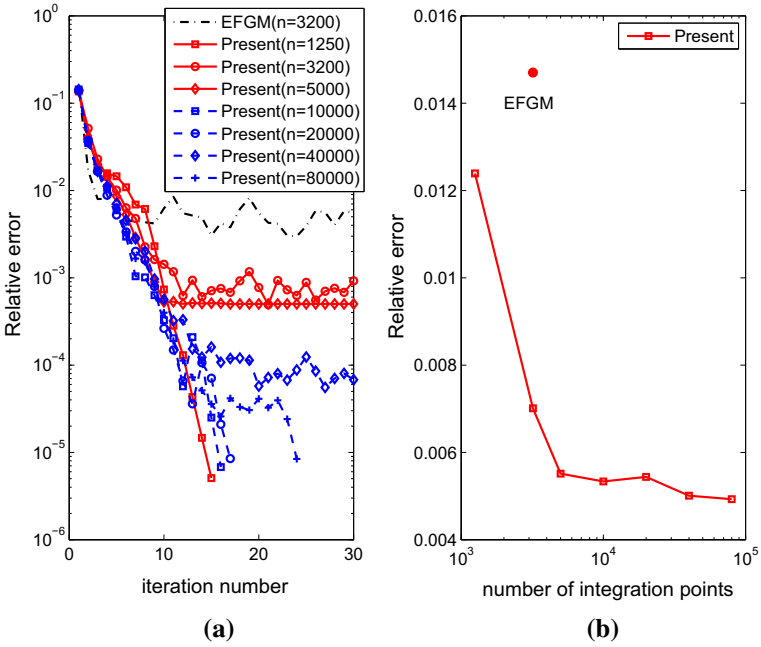

Fig. 4 **a** Convergence history; **b** relative error with different number of integration points and comparison between the present method and the EFGM

present method with the original mesh-free method, this example was solved by the EFGM, which is the most widely used mesh-free method (Li et al. 2003; Jie and Liu 2012). In this study, a 10 × 20 background mesh with 4 × 4 gauss points for each element was used for global integration in the EFGM.

The convergence history is shown in Fig. 4a. In the EFGM, numerical oscillation occurred near the iteration error 0.004. It should be mentioned that the performance of the present method, as a Monte-Carol method, possesses certain randomness. However, the convergence capability of the present method is better than the EFGM, no matter how many integration points are used. The convergence capability is especially better when the number of integration points is large.

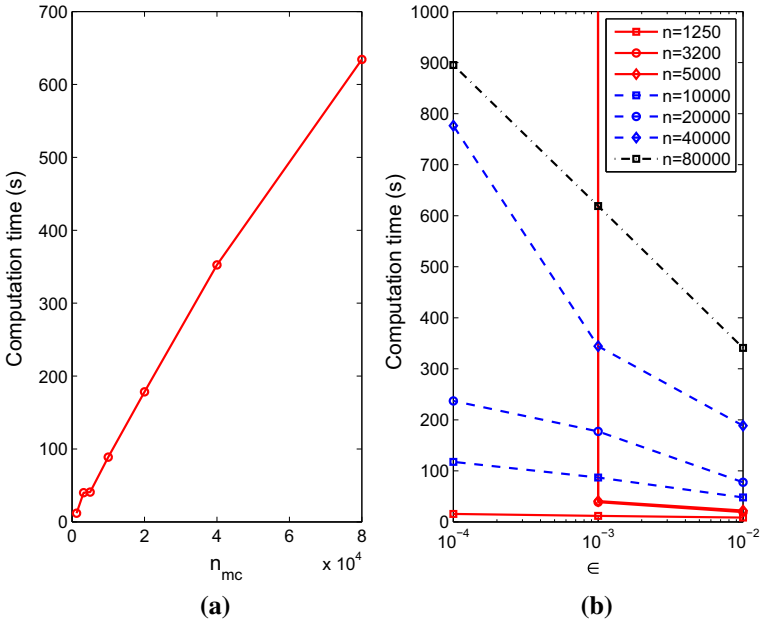

Fig. 5 **a** Influence of the parameter n_{mc} on the computation time with $\in = 0.001$; **b** Influence of the parameter $\in$ on the computation time;

By taking the convergence precision $\in = 0.001$, the average error of the phreatic surface location is shown in Fig. 4b. It can be seen that the present method can obtain higher accuracy as compared with the EFGM. The more integration points are used, the higher accuracy are obtained. However, more integration points may lead to more computation effort. From Fig. 4a, the recommended value of the convergence precision $\in$ is 0.01–0.001. From Fig. 4b, the number of integration points is suggested to be 20–100 times of the number of field nodes.

In terms of the computation cost, obviously, a Monte-Carol method can not be a high efficient method. Fig. 5a shows the influence of the parameter n_{mc} on the computation time with $\in = 0.001$, and Fig. 5b shows the influence of the parameter $\in$ on the computation time. It is found that the computation time increases near linearly with the parameter n_{mc}. This is because, as the number of field nodes is rather small, the computation time in each iteration is dominated by the global integration, rather than the solution of the global system equation. Furthermore, the computation time of the global integration depends on the number of integration points linearly. On the other hand, when the number of integration points is fixed, the computation time increases as the convergence precision $\in$ decreases. The smaller the convergence precision $\in$ is, the more iterations are needed. When the convergence precision $\in$ is taken to be too small to be achieved, the number of iterations and the computation time are infinities. Taking the same number of integration points, the comparison of the computation time between the present method and the EFGM is shown in Table 3. The average computation time for each iteration is approximately 3.33 s for the present method and 2.98 s for the EFGM. However, the convergence of the present method is better than the EFGM; that is to say, less iterations are needed given the same convergence precision $\in$. Therefore, the computation efficiency of the present method is generally better than the EFGM.

Table 3 Comparison of the computation time between the present method and the EFGM

Convergence precision ∈	EFGM		Present method	
	Number of iterations	Total computation time (s)	Number of iterations	Total computation time (s)
0.005	6	17.88	7	23.31
0.004	15	44.70	8	26.64
0.003	24	71.52	8	26.64
0.002	∞	∞	9	29.97
0.001	∞	∞	12	39.96

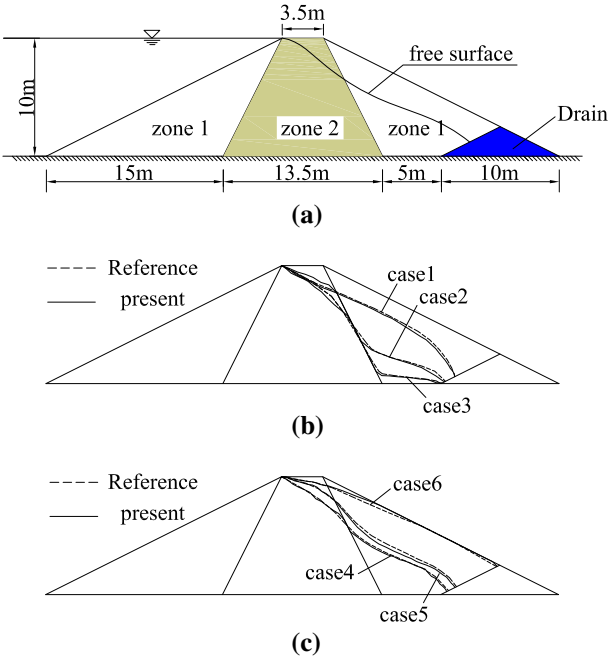

Fig. 6 **a** Seepage through inhomogeneous trapezoidal dam; **b** free surface results of cases 1–3; **c** free surface results of cases 4–6

5.2 Seepage Through Inhomogeneous Trapezoidal Dam

The seepage through an inhomogeneous anisotropic dam with trapezoidal cross section is considered. The domain of this problem is composed of three material zones. The problem is depicted in Fig. 6a. This example was chosen to prove the capability of the present method in solving seepage through inhomogeneous media with irregular geometry.

The hydraulic conductivity is assumed to be constant in each material zone, and 6 different hydraulic conductivity values are considered (see Table 4). Isotropic hydraulic conductivity is considered in the first 4 cases. Case 1 corresponds to homogeneous condition. In cases 2 and 3, the hydraulic conductivity values of zone 1 are assumed to be 10 and 100 times of that in zone 2. In the last two cases, anisotropic hydraulic conductivity is considered. In these

Table 4 Hydraulic conductivity values for different zones of the trapezoidal dam (cm/s)

	Hydraulic conductivity of zone 1		Hydraulic conductivity of zone 2	
	k_x	k_y	k_x	k_y
Case 1	1	1	1	1
Case 2	1	1	0.1	0.1
Case 3	1	1	0.01	0.01
Case 4	1	1	0.25	0.25
Case 5	4	1	1	0.25
Case 6	16	1	4	0.25

cases, the hydraulic conductivity of zone 1 is four times of zone 2 and the ratios of hydraulic conductivity in the x-direction over that in y-direction are, respectively, 4 and 16.

The Monte Carlo integration points and initial and final nodal distributions are shown in Fig. 7. The nodal distance in each direction is 0.5 m. The number of integration points n_{mc} in Eq. (32) was taken to be 20,000, approximately 20 times of the number of field nodes. and the convergence precision $\in$ in Eq. (29) was taken to be 0.01.

The results obtained by the present method are compared with Kazemzadeh-Parsi and Daneshmand (2012) in Fig. 6b, c. Good agreement can be seen from these figures. Thus, the capability of the present method in solving seepage through inhomogeneous media with irregular geometry is validated.

5.3 Transient Seepage Through a Sandbox

The computational formulations developed in this paper are applicable to transient seepage problems as well. In this example, transient seepage through a sandbox is considered.

As the first case, the sandbox is homogeneous. The length is 3.15 m, and the height is 0.33 m. The hydraulic conductivity is 0.33 cm/s, the specific storage is 0, and the specific yield is 0.18. The initial water level in the sand box is 0.1 m. At the time $t = 0\,s$, the water level at the upstream surface suddenly rises from 0.1 to 0.3 m, while the downstream water level is kept constant at 0.1 m (Fig. 8).

This example has been investigated through the laboratory test by Akai et al. (1977). In the laboratory test, a steel water channel, the size of which was 4.0 m in length, 0.25 m in width and 0.50 m in height, was utilized. The both sides of the water channel were connected with water pipes to control the water level in time. The sand sample was in the middle of the water channel, the size of which was 3.15 m in length, 0.23 m in width and 0.33 m in height. At the bottom of the water channel, a number of water pressure gauges were installed, the spacing of which was 0.2 m. The water pressure was measured by the water pressure gauge, and thus the phreatic surface heights at the gauge locations were obtained. Using these discrete data of phreatic surface, Akai et al. (1977) finally proposed the phreatic surface in the form of continuous curves, and we digitized these curves from the original paper for comparison.

The Monte Carlo integration points and initial and final nodal distributions are shown in Fig. 9. The nodal distance in each direction is 0.03 m. The number of integration points n_{mc} in Eq. (32) was taken to be 50,000, approximately 50 times of the number of field nodes and the convergence precision $\in$ in Eq. (29) was taken to be 0.01.

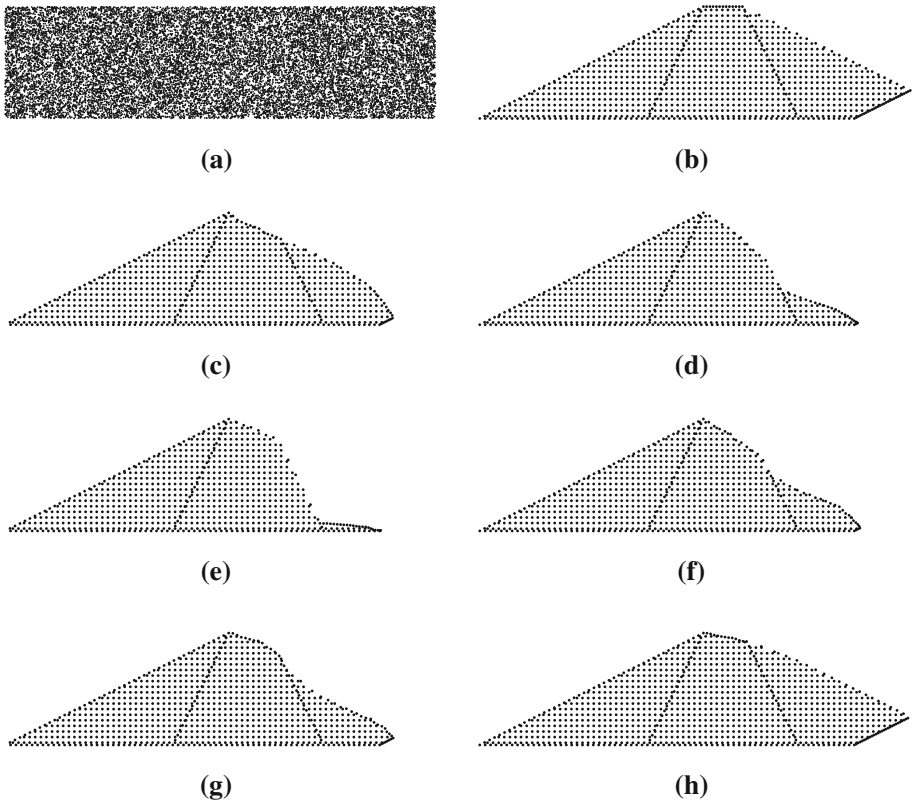

Fig. 7 **a** Monte Carlo integration points; **b** initial nodal distribution; **c**–**h** final nodal distribution of cases 1–6

The phreatic surfaces at various time steps from the present numerical method and the laboratory test are plotted in Fig. 8. A comparison between the numerical results and laboratory results has proved the effectiveness of the present method for transient seepage problem.

As the second case, the inhomogeneous media is considered. The hydraulic conductivity is given as 0.33 cm/s for $x < 1.5$ and 1.65 cm/s elsewhere. The other parameters are the same with the first case. The Monte Carlo integration points and initial and final nodal distributions are shown in Fig. 11.

The phreatic surfaces at various time steps for the inhomogeneous case and the homogeneous case are plotted in Fig. 10. It can be seen that due to that the permeability is stronger for $x \geq 1.5$, the water level rises slower than the homogeneous case. Obvious twists occur at the material interface. The contrast between the inhomogeneous and homogeneous cases follows the general rule. Thus, the capability of the present method in solving transient seepage through homogeneous and inhomogeneous media is proved (Fig. 11).

6 Conclusions

In this work, a novel mesh-free approach is proposed for the analysis of unconfined seepage problems. In this approach, the shape functions are constructed by the moving Kriging

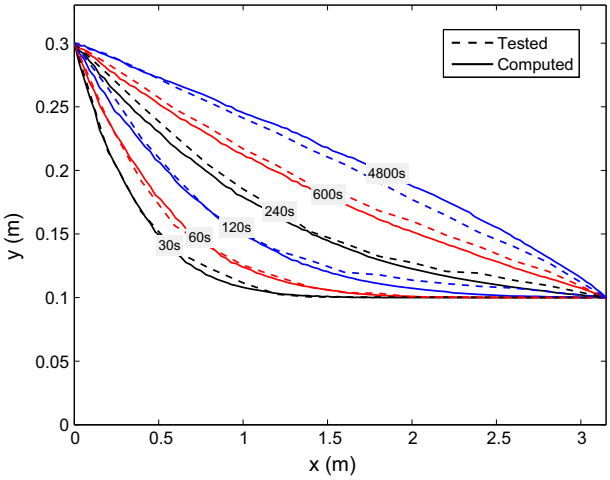

Fig. 8 Phreatic surfaces at various time steps from the present numerical method and the laboratory test

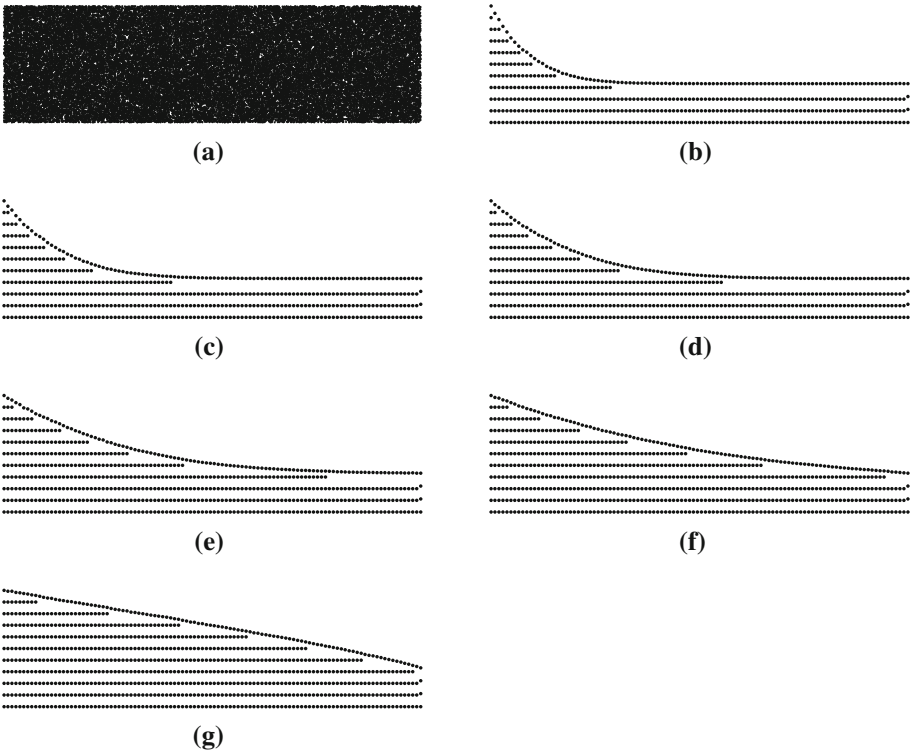

Fig. 9 **a** Monte Carlo integration points; **b** initial nodal distribution; **c**–**g** final nodal distribution at various time steps for the homogeneous case

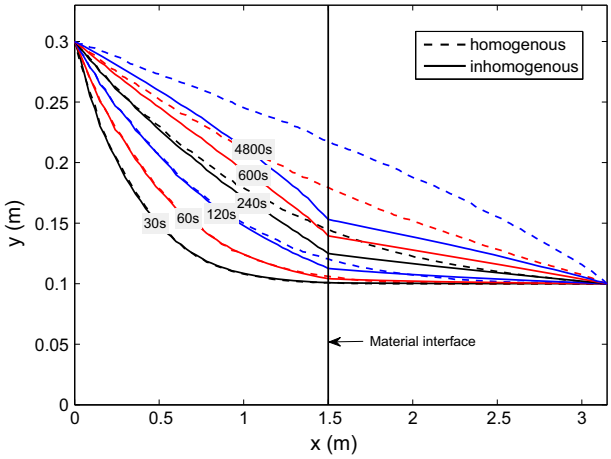

Fig. 10 Phreatic surfaces at various time steps for the inhomogeneous and homogeneous cases

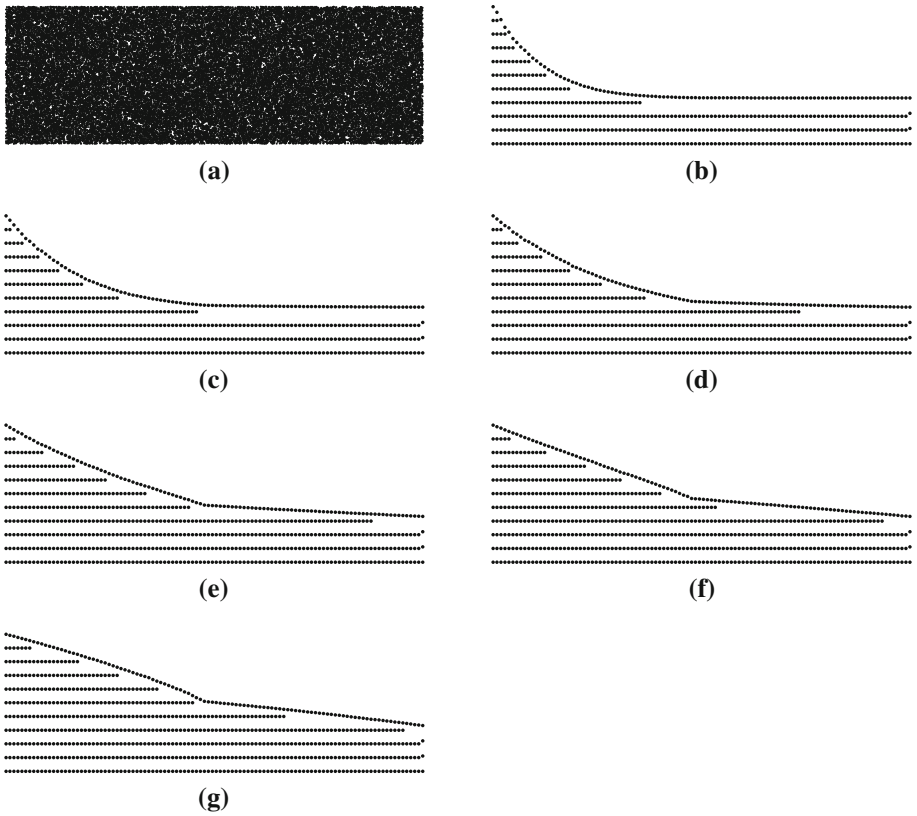

Fig. 11 **a** Monte Carlo integration points; **b** initial nodal distribution; **c–g** final nodal distribution at various time steps for the inhomogeneous case

interpolation, so the essential boundary conditions can be implemented directly. The global numerical integration is directly performed by the Monte Carlo integration, which is especially suitable for complicated moving phreatic boundary. The benchmark examples verified the correctness and convenience of the present method. The main conclusions can be summarized as follows:

(1) The present method is a true mesh-free method, which does not require a mesh for either shape function construction or numerical integration. Another important advantage of the present method is the convenient numerical implementation.
(2) Compared with the original mesh-free method, the present method can achieve better convergence and higher accuracy with rational computation cost.
(3) According to the numerical example, the number of integration points is suggested to be 20–100 times of the number of field nodes.
(4) A corresponding procedure for handling material discontinuity is presented, which extends the approach to the inhomogeneous medium seepage problems.
(5) The present method is proved to be suitable for the analysis of transient seepage through homogeneous and inhomogeneous media, through a comparison with a laboratory test.
(6) This study focuses on the analysis of two-dimensional problems. However, since both the interpolation and integration methods are dimensionless, the present method can be thus extended to three-dimensional problems in engineering practice.

Acknowledgements The research is supported by the National Natural Science Foundation of China (NSFC) through Grant Nos. 41530638, 41372302 and High Level Talent Project in Guangdong Province through Grant No. 20143900042010003.

References

Akai, K., Ohnishi, Y., Nishigaki, M.: Finite element analysis of saturated–unsaturated seepage flow in soils. Proc. Jpn. Soc. Civil Eng. **264**, 87–96 (1977)
Bardet, J.P., Tobita, T.: A practical method for solving free-surface seepage problems. Comput. Geotech. **29**(6), 451–475 (2002)
Bathe, K.J., Khoshgoftaar, M.R.: Finite element free surface seepage analysis without mesh iteration. Int. J. Numer. Anal. Methods Geomech. **3**, 13–22 (1979)
Belytschko, T., Lu, Y.Y., Gu, L.: Element-free Galerkin methods. Int. J. Numer. Methods Eng. **37**(2), 229–256 (1994)
Belytschko, T., Krongauz, Y., Organ, D., et al.: Meshless methods: an overview and recent developments. Comput. Methods Appl. Mech. Eng. **139**(1), 3–47 (1996a)
Belytschko, T., Krongauz, Y., Fleming, M., et al.: Smoothing and accelerated computations in the element free Galerkin method. J. Comput. Appl. Math. **74**(12), 111–126 (1996b)
Chaiyo, K., Rattanadecho, P., Chantasiriwan, S.: The method of fundamental solutions for solving free boundary saturated seepage problem. Int. Commun. Heat Mass Transf. **38**(2), 249–254 (2011)
Chen, J.T., Hsiao, C.C., Chiu, Y.P., et al.: Study of free-surface seepage problems using hypersingular equations. Commun. Numer. Methods Eng. **23**(8), 755–769 (2007)
Cheng, Y.M., Tsui, Y.: Technical note: an efficient method for the free surface seepage flow problems. Comput. Geotech. **15**(1), 47–62 (1993)
Crowe, A.S., Shikaze, S.G., Schwartz, F.W.: A grid generating algorithm for simulating a fluctuating water table boundary in heterogeneous unconfined aquifers. Adv. Water Resour. **22**(6), 567–575 (1999)
Darbandi, M., Torabi, S.O., Saadat, M., et al.: A moving-mesh finite-volume method to solve free-surface seepage problem in arbitrary geometries. Int. J. Numer. Anal. Methods Geomech. **31**(14), 1609–1629 (2007)
Desai, C.S.: Finite element residual schemes for unconfined flow. Int. J. Numer. Methods Eng. **10**, 1415–1418 (1976)
Desai, C.S., Li, G.C.: A residual flow procedure and application for free surface flow in porous media. Adv. Water Resour. **6**, 27–35 (1983)

Frolkovi, P.: Application of level set method for groundwater flow with moving boundary. Adv. Water Resour. **47**(10), 56–66 (2012)
Gioda, G., Gentile, C.: A nonlinear programming analysis of unconfined steady-state seepage. Int. J. Numer. Anal. Methods Geomech. **11**(3), 283–305 (1987)
Gu, L.: Moving Kriging interpolation and element-free Galerkin method. Int. J. Numer. Methods Eng. **56**, 1–11 (2003)
Hashemi, M.R., Hatam, F.: Unsteady seepage analysis using local radial basis function-based differential quadrature method. Appl. Math. Model. **35**(10), 4934–4950 (2011)
Hornung, U., Krueger, T.: Evaluation of the Polubarinova-Kochina Formula for the dam problem. Water Resour. Res. **21**, 395–398 (1985)
Jie, Y., Jie, G., Mao, Z., et al.: Seepage analysis based on boundary-fitted coordinate transformation method. Comput. Geotech. **31**(4), 279–283 (2004)
Jie, Y.X., Liu, Y.: Simulated annealing based algorithm for node generation in seepage analysis with meshless method. Mech. Res. Commun. **43**, 96–100 (2012)
Jie, Y.X., Fu, X.D., Deng, G.: Treatment of transitional element with the Monte Carlo method for FEM-based seepage analysis. Comput. Geotech. **52**(10), 1–6 (2013)
Kazemzadeh-Parsi, M.J., Daneshmand, F.: Unconfined seepage analysis in earth dams using smoothed fixed grid finite element method. Int. J. Numer. Anal. Methods Geomech. **36**(6), 780–797 (2012)
Kazemzadeh-Parsi, M.J., Daneshmand, F.: Three dimensional smoothed fixed grid finite element method for the solution of unconfined seepage problems. Finite Elem. Anal. Des. **64**(3), 24–35 (2013)
Lam, L., Fredlund, D.G.: Saturated–unsaturated transient finite element seepage model for geotechnical engineering. Adv. Water Resour. **7**, 132–136 (1984)
Lam, L., Fredlund, D.G., Barbour, S.L.: Transient seepage model for saturated–unsaturated soil systems: a geotechnical engineering approach. Can. Geotech. J. **24**(4), 565–580 (1987)
Leontiev, A., Huacasi, W.: Mathematical programming approach for unconfined seepage flow problem. Eng. Anal. Bound. Elem. **25**(1), 49–56 (2001)
Li, G.X., Ge, J.H., Jie, Y.X.: Free surface seepage analysis based on the element-free method. Mech. Res. Commun. **30**(1), 9–19 (2003)
Obnosov, Y.V., Kacimov, A.R., Castro-Orgaz, O.: Analytical solutions for steady phreatic flow appearing/re-emerging toward/from a Bedrock/Caprock Isobaric Breach: the Polubarinova-Kochina–Numerov and Pavlovsky problems revisited. Transp. Porous Media **109**(2), 1–22 (2015)
Organ, D., Fleming, M., Terry, T., et al.: Continuous meshless approximations for nonconvex bodies by diffraction and transparency. Comput. Mech. **18**(3), 225–235 (1996)
Rafiezadeh, K., Ataie-Ashtiani, B.: Transient free-surface seepage in three-dimensional general anisotropic media by BEM. Eng. Anal. Bound. Elem. **46**(3), 51–66 (2014)
Shahrokhabadi, S., Toufigh, M.M.: The solution of unconfined seepage problem using natural element method (NEM) coupled with genetic algorithm (GA). Appl. Math. Model. **37**(5), 2775–2786 (2013)
Sharif, N.H., Wiberg, N.E.: Adaptive ICT procedure for non-linear seepage flows with free surface in porous media. Commun. Numer. Methods Eng. **18**(3), 161–176 (2002)
Zhang, J.H., Xu, Q.J., Chen, Z.Y.: Seepage analysis based on the unified unsaturated soil theory. Mech. Res. Commun. **28**(1), 107–112 (2001)
Zheng, H., Liu, D.F., Lee, C.F., et al.: New variational inequality formulation for seepage problems with free surfaces. Appl. Math. Mech. **26**(3), 396–406 (2005)
Zheng, B., Dai, B.: A meshless local moving Kriging method for two-dimensional solids. Appl. Math. Comput. **218**(2), 563–573 (2011)
Zheng, H., Liu, F., Li, C.: Primal mixed solution to unconfined seepage flow in porous media with numerical manifold method. Appl. Math. Model. **39**(2), 794–808 (2015)